DIRECT NUMERICAL SIMULATION OF HIGH ASPECT RATIO SPANWISE-ALIGNED BARS

M. MacDonald, A. Ooi, N. Hutchins & D. Chung

Department of Mechanical Engineering
University of Melbourne
Victoria 3010, Australia
michael.macdonald@unimelb.edu.au

ABSTRACT

We conduct minimal-channel direct numerical simulations of turbulent flow over two-dimensional rectangular bars aligned in the spanwise direction. This roughness has been often described as d-type, as the roughness function ΔU^+ is thought to depend only on the outer-layer length scale (pipe diameter, channel half height or boundary layer thickness). This is in contrast to conventional engineering rough surfaces, named k-type, for which ΔU^+ depends on the roughness height, k. The minimal-span rough-wall channel is used to circumvent the high cost of simulating high Reynolds number flows, enabling a range of bars with varying aspect ratios to be investigated. The present results show that increasing the trough-to-crest height (k) of the roughness while keeping the width between roughness bars, $\mathcal{W}$, fixed in wall units, results in non-k-type behaviour. The roughness function appears to scale with $\mathcal{W}$, suggesting that this is the only relevant parameter for very deep rough surfaces with $k/\mathcal{W} \gtrsim 3$. In these situations, the flow no longer has any information about how deep the roughness is and instead can only 'see' the width of the fluid gap between the bars.

INTRODUCTION

Turbulent flows bounded by a rough wall are ubiquitous in engineering and geophysical applications. The roughness generally increases the drag force exerted on the wall when compared to a smooth wall, which is often quantified by the (Hama) roughness function, ΔU^+ (Hama, 1954). This quantity reflects the retardation of the mean streamwise flow over a rough wall compared to a smooth wall, and can be related to the difference in skin-friction coefficients, C_f. The superscript $+$ indicates quantities non-dimensionalised on kinematic viscosity ν and friction velocity $U_\tau \equiv \sqrt{\tau_w/\rho}$, where τ_w is the wall-shear stress and ρ is the fluid density. The intuition that increasing the roughness height would increase the drag suggests that the roughness function should scale on some characteristic roughness height k^+. In the fully rough regime, in which the skin-friction coefficient no longer depends on the Reynolds number, the roughness function scales as $\Delta U^+ = \kappa^{-1}\log(k^+) + D$, where $\kappa \approx 0.4$ is the von Kármán constant and D depends on the rough surface in question (Hama, 1954). These surfaces have been termed k-type roughness, due to the dependence on the roughness height. However, a second type of rough-wall flow was discovered for closely packed rectangular bars aligned in the spanwise direction in pipes (Streeter & Chu, 1949; Sams, 1952; Ambrose, 1956). This was discussed in the seminal work by Perry *et al.* (1969), who studied these spanwise-aligned bars in a developing turbulent boundary layer. Here, the roughness function was shown to not scale on the roughness height k^+, but rather the boundary layer height, δ^+, as $\Delta U^+ = \kappa^{-1}\log(\delta^+) + A$. Perry *et al.* (1969) termed this roughness d-type roughness (named after the pipe diameter, due to the earlier pipe flow studies), as it depends on the outer-layer length scale (pipe diameter, boundary layer thickness or channel half height, h).

The flow physics on how the outer-layer length scale influences ΔU^+ is unclear. Authors such as Perry *et al.* (1969), Cui *et al.* (2003) and Coleman *et al.* (2007) suggested that there are stable vortices inside the roughness cavities which are isolated from the flow above. The flow within the roughness canopy (below the roughness crest) would therefore be similar to a lid-driven cavity flow, while the outer-flow would see what is similar to an alternating slip and no-slip boundary condition at the interface. The outer-layer flow would have no information about how deep the cavities are, implying k is not relevant. Townsend (1976), Djenidi *et al.* (1999) and Jiménez (2004) proposed some form of ejection of the roughness cavity flow into the outer layer, where these ejections are triggered by an outer-layer-dependent process such as large-scale sweeps, which scales with d.

Much of the difficulty in studying d-type roughness comes from experimental uncertainty in determining U_τ. An incorrect measure of this quantity directly influences $\Delta U^+ \equiv \Delta U/U_\tau$, which can make isolating the effects of k and h problematic. Jiménez (2004) reviewed several experimental studies of d-type rough surfaces but found that the evidence for the idea that ΔU^+ only scales on h was uncertain. Conventional direct numerical simulations provide an exact estimate of U_τ, but the closely packed nature of the spanwise aligned bars necessitates an extremely dense grid. Leonardi *et al.* (2007) provided one of the first direct numerical simulations (DNS) of a d-type surface. These authors were not able to verify if ΔU^+ was a function of the channel half-height h, but did show that ΔU^+ was not a function of the roughness height k^+. They therefore broadened the definition of d-type roughness to be any surface for which $\Delta U^+ \neq f(k^+)$.

The aforementioned expense of the dense grid has made simulating d-type roughness infeasible for many researchers. However, recently it was shown in Chung *et al.* (2015) and MacDonald *et al.* (2017) that a minimal-span channel can be used to directly simulate rough-wall flows, which follows on from the early work of Jiménez & Moin (1991) and Hamilton *et al.* (1995) in smooth-wall minimal domains. This technique involves restricting the spanwise domain width, L_y, to be much smaller than the channel half height, h, with $L_y^+ \sim O(100)$ typical. Only the near-wall flow around the roughness is fully resolved while the outer-layer flow is restricted by the narrow domain. As a result, the mean velocity profile of the minimal-span channel deviates from the full-span channel above a wall-normal critical height $z_c \approx 0.4L_y$. Below z_c, the turbulent flow is the same as in a full-span channel, so is regarded as 'healthy' turbulence (Flores & Jiménez, 2010). MacDonald *et al.* (2016) successfully used this technique to simulate densely packed sinusoidal surfaces with solidities (frontal roughness area divided by plan area) of up to $\Lambda = 0.54$. Given that d-type surfaces usually have $\Lambda \geq 0.5$ (Jiménez, 2004), then the minimal-span channel would be highly suitable for such surfaces. As there is explicitly no outer-layer length scale associated with the flow (as there are no outer-layer length scale eddies) in the minimal channel framework, we cannot

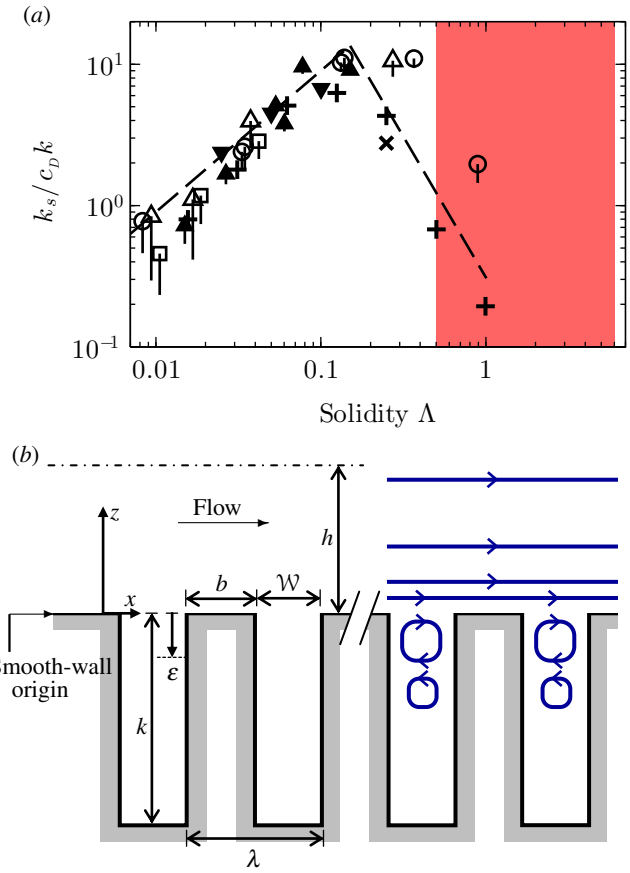

Figure 1. (*a*) Equivalent sand grain roughness against solidity for different rough surfaces, adapted from Jiménez (2004). The solidity of the present rough surfaces ranges over $0.5 \leq \Lambda \leq 6$, shown by the red region. (*b*) Sketch of the present roughness. In all cases, $\mathcal{W} = b = \lambda/2$. Virtual origin (Jackson, 1981) denoted by ε. Blue arrows show streamlines commonly used to describe *d*-type roughness.

explicitly test the hypothesis that $\Delta U^+ = f(h^+)$. However, by increasing the channel width and therefore the largest captured length scale z_c, this can serve as a span-independence verification to provide some indication on the influence of the largest length scale in the flow. Moreover, if we consider several rough surfaces with varying k^+ then we can examine what functional dependence, if any, ΔU^+ has on k^+.

Most previous *d*-type roughness studies use square bars aligned in the spanwise direction, and vary the width of the fluid gap between the bars, $\mathcal{W}$, for a fixed k (Djenidi *et al.*, 1999; Cui *et al.*, 2003; Coleman *et al.*, 2007; Leonardi *et al.*, 2007). The present study varies k for fixed values of $\mathcal{W}$, which corresponds to progressively taller rectangular bars. The solidity, $\Lambda = k/(2\mathcal{W})$, is exceptionally large, with values of 0.5 up to 6. Figure 1(*a*) shows the equivalent sand grain roughness plotted against solidity for different rough surfaces, adapted from Jiménez (2004). The solidity of the rough surfaces in the present study is indicated by the red region, and can be seen to have much larger aspect ratios than previous studies. The sketch in figure 1(*b*) of the present roughness shows the flow patterns often used to describe *d*-type roughness (Jiménez, 2004). Intuitively, the vortices inside the roughness cavities would likely scale on the cavity width $\mathcal{W}^+$ which could suggest some kind of $\Delta U^+ = f(\mathcal{W}^+)$ dependence. Rather than create a new '$\mathcal{W}$-type' roughness classification, we will follow Leonardi *et al.* (2007) and continue to use the term *d*-type roughness, to refer to a surface where $\Delta U^+ \neq f(k^+)$.

Table 1. Description of the simulations performed. Symbols: $\mathcal{W}$, distance between bars; k, peak-to-trough roughness height; $\Lambda = k/(2\mathcal{W})$, solidity; N_x, number of cells in streamwise direction; N_{zk}, number of cells in the wall-normal direction below the roughness crest; U_{bf}^+, expected full-span bulk velocity using a composite velocity profile; ΔU^+, roughness function. All simulations conducted at $Re_\tau \approx 395$ with $L_x^+ = 1000$, $\Delta y^+ \approx 4.5$, and wall-normal grid spacings at the roughness crest and channel centre of $\Delta z_w^+ \approx 0.4$ and $\Delta z_h^+ \approx 12.9$, respectively.

$\mathcal{W}^+$	k^+	Λ	L_y^+	N_x	N_{zk}	U_{bf}^+	ΔU^+
10	5	0.25	153	1600	12	16.7	0.9
10	10	0.5	153	1600	24	16.1	1.5
10	20	1.0	153	1600	48	15.6	2.0
10	30	1.5	153	1600	72	15.2	2.5
10	40	2.0	153	1600	96	15.1	2.6
10	60	3.0	153	1600	144	15.1	2.6
20	60	1.5	153	800	144	15.0	2.7
20	120	3.0	153	800	195	14.8	2.8
50	150	1.5	306	320	360	14.4	3.3
50	300	3.0	306	320	720	14.4	3.2
100	50	0.25	306	320	112	13.6	4.0
100	150	0.75	306	320	229	12.9	4.4
100	300	1.5	306	320	302	12.6	4.5
100	600	3.0	306	320	452	12.6	4.5
100	1200	6.0	306	320	752	12.5	4.6
100	300	1.5	612	320	302	13.2	4.8

METHODOLOGY

The numerical method used in this study is described and validated in Chan *et al.* (2015) and MacDonald *et al.* (2016) This is a second-order finite volume code which directly solves the Navier–Stokes equations. A half-height (open) channel is used whereby a slip wall was positioned at $z = h$, while a no-slip impermeable wall is used for the spanwise-aligned bars. Periodic boundary conditions are applied in the streamwise and spanwise directions. The flow is driven by a prescribed constant mass flux, so that the driving pressure gradient of the channel, $G_x = -\mathrm{d}P/\mathrm{d}x$, varies at each time step. This mass flux is set via trial and error such that the friction Reynolds number, $Re_\tau = U_\tau h/\nu \approx 395$ for all cases. This Reynolds number was selected as it was shown in Chan *et al.* (2015) that the roughness function, ΔU^+, is overestimated for $Re_\tau = 180$ simulations, becoming Reynolds number invariant for $Re_\tau \gtrsim 395$. Table 1 details the simulations that were performed in this study. The expected full-span bulk velocity, $U_{bf}^+ = \int U_{comp}^+ \mathrm{d}z^+/h^+$, is given, where the composite velocity profile of Nagib & Chauhan (2008) for full-span channel flow is fitted to the simulation data for $z > z_c$ to give U_{comp}^+.

A cell-to-cell expansion ratio of approximately 1.028 is used in the wall-normal direction above the roughness crest, resulting in a fairly large grid spacing at the channel centreline. However, the grid spacings below z_c are such that Δz^+ only increases beyond conventional DNS spacings above the wall-normal critical height, z_c. As

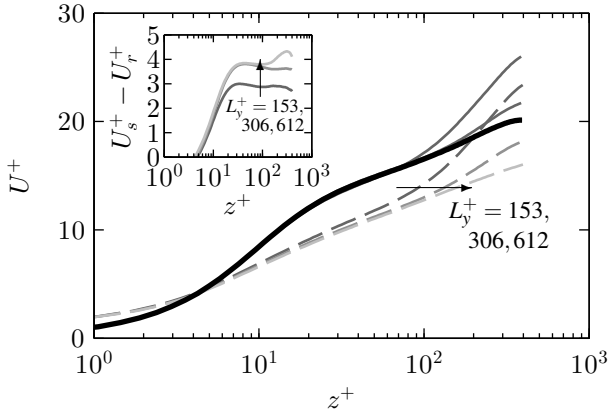

Figure 2. Mean velocity profile for smooth-wall (solid) and rough-wall (dashed) minimal channels with $\mathcal{W}^+ \approx 100$, $k^+ \approx 300$. Lighter grey refers to increasing channel width (table 1). Thick black line is full-span smooth-wall channel data of Moser *et al.* (1999). Inset shows difference in smooth- and rough-wall velocity. The origin in z^+ is at the roughness crest.

the region of the flow above z_c is already altered due to the nature of the minimal channel, these spacings should have negligible impact on the near-wall flow of interest. The wall-normal mesh spacing below the roughness crest is approximately constant at Δz_w^+ for cases with $k^+ < 120$. Cases with larger k^+ have a larger wall-normal spacing towards the centre of the roughness cavity, with $\Delta z^+ \approx 2$, however at the roughness crest and trough it is $\Delta z^+ \approx 0.4$.

The minimal-span channel is used so that the streamwise and spanwise domain sizes are relatively small compared to conventional (full-span) channels. The recommendation in Chung *et al.* (2015) is typically used to determine the spanwise domain width for k-type roughness, namely $L_y \gtrsim \max(100\nu/U_\tau, k/0.4, \lambda_{r,y})$, where $\lambda_{r,y}$ is a characteristic roughness spanwise length scale. For the present two-dimensional roughness, $\lambda_{r,y} \to \infty$ and it is likely that another length scale would take precedence, anticipated to be $\mathcal{W}$ for $\mathcal{W} \ll k$. This $\lambda_{r,y}$ constraint will therefore be ignored. The second constraint comes from ensuring the roughness is submerged in healthy turbulence i.e. $k < z_c = 0.4L_y$. Given that this is likely more applicable for k-type roughness and the present roughness may be more dependent on $\mathcal{W}$, we will instead ensure $L_y > O(\mathcal{W})$, where the independence of the flow below z_c that sets ΔU^+ is more closely examined in the next section. The streamwise length should satisfy $L_x \gtrsim \max(3L_y, 1000\nu/U_\tau, \lambda_{r,x})$ (MacDonald *et al.*, 2017), where for the present roughness with relatively narrow streamwise wavelengths of $\lambda_{r,x}^+ \leq 200$, the second constraint is the limiting one.

RESULTS

Effect of channel width

The flow of the minimal-span channel is intrinsically related to the spanwise width, with the critical wall-normal height scaling as $z_c = 0.4L_y$. Previous studies support the view that the roughness crest must be submerged in healthy turbulence, requiring $z_c^+ > k^+ \Rightarrow L_y^+ > k/0.4$ (Chung *et al.*, 2015). For the present roughness, where it is presumed k is not a relevant scale, this relationship must be re-examined. Figure 2 shows the effect of increasing channel width on the mean velocity profile for bar roughness with $\mathcal{W}^+ \approx 100$, $k^+ \approx 300$. As observed in previous minimal-span channels, increasing the channel width L_y^+, and hence critical height z_c, reduces the centreline velocity in the altered outer layer. A larger proportion of energy containing eddies are captured by the wider channels and the results tend to match more closely with conventional full-span channel flow.

The rough-wall flow with the smallest width of $L_y^+ = 153 \approx 1.5\mathcal{W}^+$ (dark grey dashed line) is seen to result in a slightly increased mean velocity below the critical height of $z_c^+ \approx 0.4L_y^+ \approx 61^+$, when compared to the larger width cases. This is not observed in the smooth-wall flow (solid lines) so that the velocity difference between smooth- and rough-wall flows is about 1 friction velocity lower for $L_y^+ = 153$ (inset of figure 2). When $L_y^+ \geq 306 \approx 3\mathcal{W}^+$, little difference is seen with increasing channel width. Note that there is no smooth-wall minimal-span data for $L_y^+ = 612$; instead the full-span data of Moser *et al.* (1999) is used. This may explain the increase in the velocity difference for $z^+ \gtrsim 100$ for $L_y^+ = 612$. However, the near-wall agreement in the velocity difference (inset) for $L_y^+ \gtrsim 306$ supports the view that there is little effect in increasing channel width above $L_y \geq 3\mathcal{W}$. That is, we have obtained a ΔU^+ that is insensitive to the minimal span. In terms of the critical wall-normal height, z_c, the above results suggest that for spanwise bar roughness $z_c \approx 1.2\mathcal{W}$, or that the height of the healthy turbulence region must be greater than the fluid width between bars, $\mathcal{W}$.

The classical description of d-type roughness is that the roughness function scales on the largest turbulent length scale, which is conventionally the channel half height, h. In minimal-span channels the critical height z_c can be regarded as the largest captured turbulent length scale in the flow as opposed to h. The above results, however, show that increasing z_c above $1.2\mathcal{W}$ has diminishing influence on the flow. This is therefore inconsistent with the classical description of d-type roughness being influenced by the largest length scales present in the flow.

Mean flow statistics

Streamlines of time-averaged velocity are shown in figure 3 over a contour of the wall-normal turbulence intensity, $w'^+{}^2$. Firstly, we will just consider the effect of increasing k^+ for a fixed $\mathcal{W}^+ = 10$ (figure 3*a*). Streamlines are only shown for motions with a local velocity greater than 0.05 friction velocities. A clear difference for $k^+ = 5$ is seen, with the small roughness height flattening the recirculating 'bubble'. There is a subtle difference with $k^+ = 10$, however once $k^+ \gtrsim 20$ little effect is seen with increasing k^+. This suggests that once $k/\mathcal{W} \gtrsim 2$ there is very little effect in changing k. At this point, there is a single recirculating spanwise bubble rotating in the clockwise direction. The contour shows that the turbulent motions do not penetrate far into into the roughness canopy, tending to zero within 10 to 20 viscous units. Note that these fluctuations are defined using the triple decomposition of $w = W + \widetilde{w} + w'$ (Finnigan, 2000) where the time-independent (spatially dependent) component, $\widetilde{w}$, of the fluctuation is subtracted off and w' is a purely turbulent fluctuation.

Increasing the width of the fluid gap whilst retaining a fixed aspect ratio $k/\mathcal{W}$ (figure 3*b*) results in a strengthening of the fluid recirculation region, as well as a greater penetration of the turbulence into the roughness canopy in terms of z^+. However, it still appears that the turbulent fluctuations do not penetrate much past $z/\mathcal{W} \approx 2$. When $\mathcal{W}^+ = 100$, a secondary recirculating bubble (with localised velocity greater than 0.05 friction velocities) emerges below the primary one. This secondary recirculating bubble is nearly the same strength as the primary recirculating bubble seen when $\mathcal{W}^+ = 10$ in (*a*). This secondary bubble is still present for $\mathcal{W}^+ < 100$, however its strength is substantially diminished.

A common issue in roughness studies is determining the location of the origin in z, often termed the virtual origin, ε. A physically appealing method that is often employed is to define ε as the centroid of the moment of the drag forces acting on the rough wall (Jackson, 1981). This takes the form of $\varepsilon = \int z|F_p + F_\nu| \, \mathrm{d}z / \int |F_p + F_\nu| \, \mathrm{d}z$. Figure 4(*a*) shows the ratio of the pressure drag force F_p to

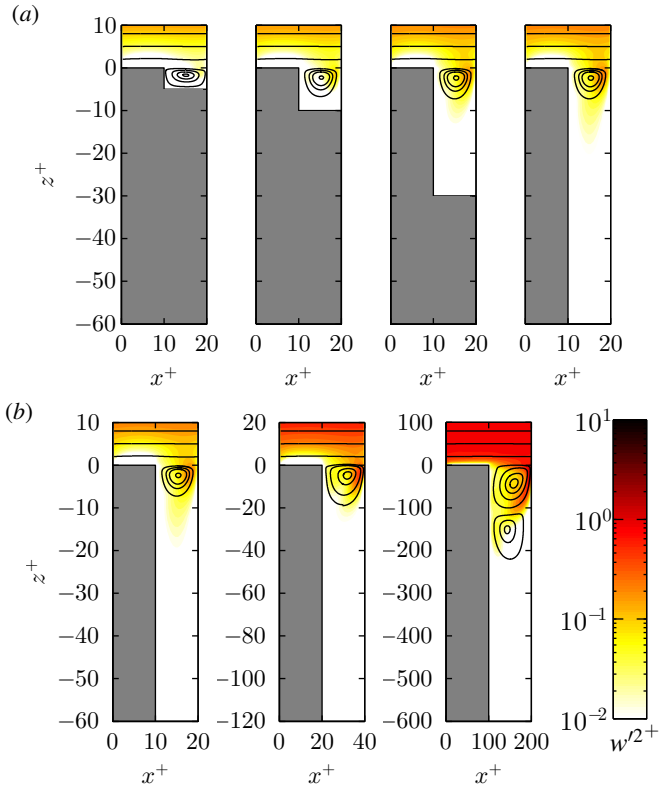

Figure 3. Streamlines of time-averaged velocity for (*a*) $\mathcal{W}^+ = 10$ with $5 \leq k^+ \leq 60$ and (*b*) $k/\mathcal{W} = 6$ with $10 \leq \mathcal{W}^+ \leq 100$. Streamlines only drawn for motions with local velocities greater than $0.05U_\tau$. Contour shows the wall-normal turbulence intensity w'^{+2} with a log colourbar.

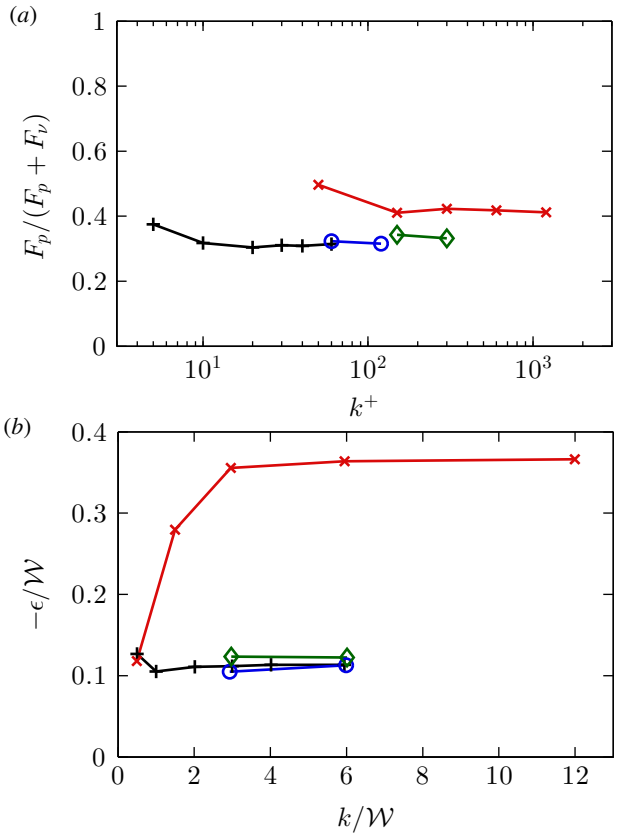

Figure 4. (*a*) Ratio of pressure to total (viscous + pressure) drag and (*b*) virtual origin ε normalised on fluid gap $\mathcal{W}$. Symbols: +, $\mathcal{W}^+ = 10$; ○, $\mathcal{W}^+ = 20$; ◇, $\mathcal{W}^+ = 50$; ×, $\mathcal{W}^+ = 100$.

the total drag force, $F_p + F_v$. For the three narrowest fluid gaps of $\mathcal{W}^+ \lesssim 50$, the pressure drag is approximately 32% of the total drag and is almost independent of k. It is only with the largest width, $\mathcal{W}^+ \approx 100$ that the pressure drag increases to around 41% of the total drag. These magnitudes are similar to those observed in three-dimensional sinusoidal roughness which exhibits *k*-type behaviour (Chan *et al.*, 2015; MacDonald *et al.*, 2016). In the seminal *d*-type work of Perry *et al.* (1969), the authors assumed that the viscous drag was negligible so that the pressure drag, which could be experimentally measured using pressure tappings, was the only contribution to U_τ. The present data for $10 \leq \mathcal{W}^+ \leq 100$ shows that the viscous drag is approximately 60–70% of the total drag, suggesting this assumption may not be ideal. However this ratio decreases with $\mathcal{W}^+$ and the values of $\mathcal{W}^+ \gtrsim 250$ used in Perry *et al.* (1969) may make the assumption more appropriate.

Figure 4(*b*) shows the virtual origin, calculated using Jackson's method. The origin for the three smallest $\mathcal{W}^+$ values is almost invariant with k, with $\varepsilon \approx 0.11\mathcal{W}$. Note that this means ε^+ increases with $\mathcal{W}^+$ however the collapse with the scaling of $\varepsilon/\mathcal{W}$ suggests $\mathcal{W}$ is a crucial parameter for the present roughness. For the largest value of $\mathcal{W}^+ \approx 100$, ε is substantially larger than the narrower cases, tending towards an asymptote of $\varepsilon \approx 0.36\mathcal{W}$ when $k/\mathcal{W} \geq 3$. This is most likely due to the secondary recirculating bubble observed in figure 3(*b*), which exists over $-200 \lesssim z^+ \lesssim -100$. This recirculating bubble causes a non-negligible pressure difference to act across the roughness elements which in turn causes ε^+ to increase. Given that this secondary bubble extends down to $z^+ \approx 200$, then it follows we require at least $k^+ > 200 \Rightarrow k/\mathcal{W} > 2$ to reach this asymptote. These results are in qualitative agreement with the high aspect ratio model of Sadique *et al.* (2017), based on flow over three-dimensional rectangular prisms. The model predicted $\varepsilon/\mathcal{W}$ to asymptote to a constant for $k/\mathcal{W} \gtrsim 5$, where it is likely the weaker sheltering behaviour of 3D roughness (Yang *et al.*, 2016) is what requires a larger $k/\mathcal{W}$ ratio to reach the asymptotic limit than the present 2D roughness.

The mean velocity profile is shown in figure 5 for the cases with $\mathcal{W}^+ = 10$ and $\mathcal{W}^+ = 100$. The velocity difference between smooth- and rough-wall flows for $\mathcal{W}^+ = 10$ (inset of figure 5*a*) has a dependence on k for $k^+ \lesssim 20$, but when k is sufficiently large ($k^+ \gtrsim 30 \Rightarrow k/\mathcal{W} \gtrsim 3$) little difference is observed. Similarly, for $\mathcal{W}^+ = 100$ a collapse is observed for $k/\mathcal{W} \gtrsim 3$ (inset of figure 5*b*), where the cases with the largest peak-to-trough heights ($k^+ = 300$, 600 and 1200) are almost indistinguishable from one another.

Roughness function

The roughness function ΔU^+ is computed by taking the value of $U_s^+ - U_r^+$ at $z_c^+ \approx 0.4L_y^+$. Figure 6(*a*) shows the roughness function against the peak-to-trough height, k^+. It is clear that increasing k^+ for fixed values of $\mathcal{W}^+$ does not tend towards the fully rough asymptote of *k*-type roughness, that is $\kappa^{-1}\log(k^+)$. However, consider fixed values of $k/\mathcal{W}$, shown by the dashed and dotted grey lines for $k/\mathcal{W} = 3$ and $k/\mathcal{W} = 6$, respectively. This is more representative of an experimental study in which a single geometry (with fixed $k/\mathcal{W}$) is studied at various flow speeds which leads to the roughness Reynolds number varying. By considering fixed $k/\mathcal{W}$, the data now appears to behave more like a *k*-type roughness in that the larger values of k^+ are tending towards the fully rough asymptote. This is despite the previous results showing very little change in the flow structures with such a large aspect ratio. It would seem that the offset constant D in $\kappa^{-1}\log(k^+) + D$ is dependent on $k/\mathcal{W}$,

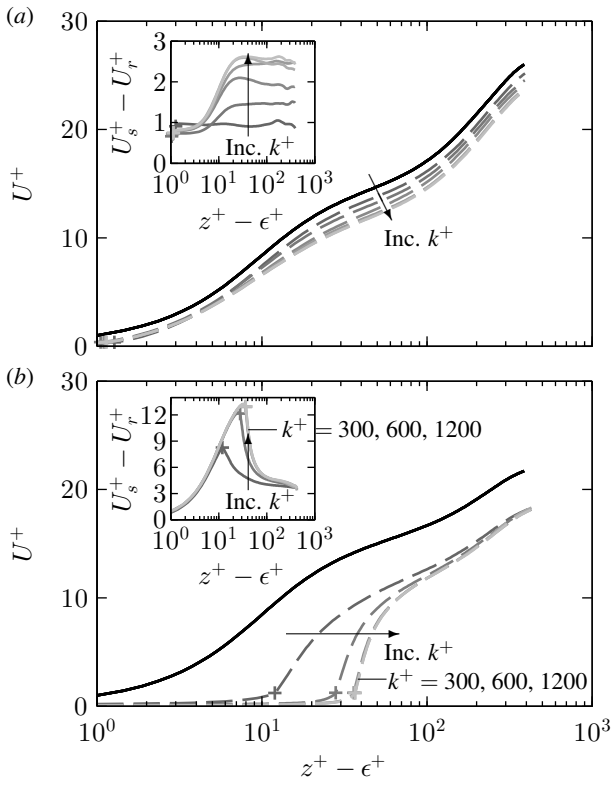

Figure 5. Mean velocity profile for smooth-wall (solid) and rough-wall (dashed) minimal channels with (*a*) $\mathcal{W}^+ \approx 10$ and $5 \le k^+ \le 60$ and (*b*) $\mathcal{W}^+ \approx 100$ and $50 \le k^+ \le 1200$. Lighter grey refers to larger k^+ (table 1). Inset shows difference in smooth- and rough-wall velocity.

with increasing $k/\mathcal{W}$ leading to a reduced D.

The roughness function as a function of solidity, $\Lambda = k/(2\mathcal{W})$ (figure 6*b*), shows how the roughness function tends towards a constant value for large solidity (large $k/\mathcal{W}$ ratios). This value depends on the fluid width $\mathcal{W}^+$, with increasing $\mathcal{W}^+$ leading to an increasing roughness function. It is important to emphasise that here we are varying k^+ for a variety of $\mathcal{W}^+$ values. Previous studies that examine the roughness function for varying solidity typically do so by keeping k^+ fixed and varying $\mathcal{W}^+$. This results in the roughness function decreasing with solidity in the so-called dense regime when $\Lambda \gtrsim 0.15$ (Jiménez, 2004; MacDonald *et al.*, 2016), as observed in figure 1(*a*). If we were to consider a fixed k^+ value for the present bar roughness and increase the wavelength, we would still obtain a reducing roughness function in the dense regime ($\Lambda \gtrsim 0.15$, shown by the vertical dashed line in figure 6*b*). To see this, consider the first data point for $\mathcal{W}^+ \approx 100$ (red cross, $k^+ \approx 50$, $\Lambda = 0.5$) and final data point for $\mathcal{W}^+ \approx 10$ (black plus, $k^+ \approx 60$, $\Lambda = 3$). Even though the roughness heights are slightly different, it is clear that the roughness function is reducing with solidity for these approximately matched k^+ values.

To better show the trend with $\mathcal{W}^+$, the roughness function is considered in figure 6(*c*) for surfaces with fixed aspect ratios of $k/\mathcal{W} = 3$ and $k/\mathcal{W} = 6$ (indicated by the dashed and dotted lines in figure 6*a*). For these fixed aspect ratio bars, the roughness function is seen to collapse on one another. This suggests that for these high aspect ratio (tall and narrow) rough surfaces, it is $\mathcal{W}$, and not k (figure 6*a*) that is the relevant length scale. The k-type asymptote, $\kappa^{-1}\log(k^+) + D$ for fixed $k/\mathcal{W}$ would then become $\kappa^{-1}\log(\mathcal{W}^+) + C$, where $C = D + \kappa^{-1}\log(k/\mathcal{W})$. If we assume the roughness function for $\mathcal{W}^+ = 100$ is in the fully rough

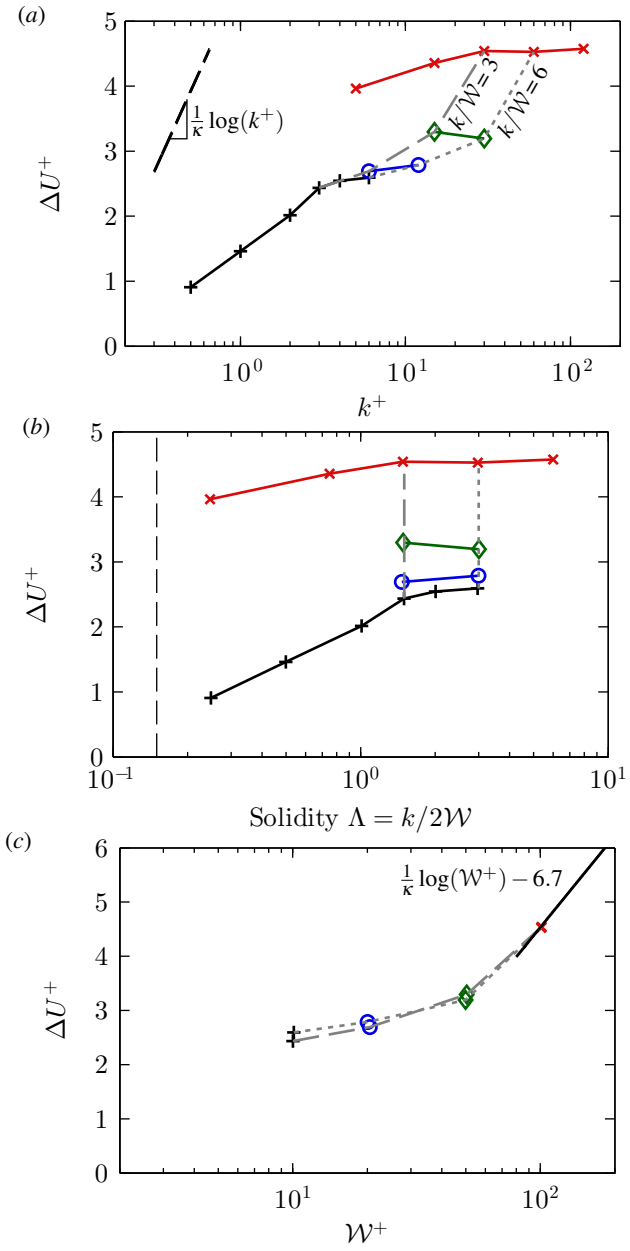

Figure 6. Roughness function, ΔU^+, plotted against (*a*) roughness height, k^+, (*b*) solidity, Λ, and (*c*) fluid gap, $\mathcal{W}^+$. Symbols: +, $\mathcal{W}^+ = 10$; ○, $\mathcal{W}^+ = 20$; ◇, $\mathcal{W}^+ = 50$; ×, $\mathcal{W}^+ = 100$. Dashed and dotted lines correspond to $k/\mathcal{W} = 3$ and $k/\mathcal{W} = 6$, respectively.

regime, then this offset C can be estimated as $C \approx -6.7$ from the present data and is independent of $k/\mathcal{W}$ (solid line in figure 6*c*). The equivalent sand grain roughness $k/k_s \equiv \exp(-\kappa(3.5 + D)) = (k/\mathcal{W})\exp(-\kappa(3.5 + C))$ can also be estimated, where the constant 3.5 comes from the difference between the smooth-wall log-law offset (≈ 5) and Nikuradse's rough-wall constant (≈ 8.5). In other words, for $k/\mathcal{W} \ge 3$ we have $k_s \approx \mathcal{W}\exp(-3.2\kappa) \approx 0.3\mathcal{W}$, or that it is solely a function of $\mathcal{W}$. For $\mathcal{W}^+ \le 100$, which is more reminiscent of the k-type transitionally rough regime, the roughness function follows a linear trend of $\Delta U^+ \approx 0.021\mathcal{W}^+ + 2.3$.

CONCLUSIONS

Direct numerical simulations of turbulent flow over spanwise-aligned bars have been performed in which the height of the bars, k, is larger than the spacing between them, $\mathcal{W}$. These bars are some-

times referred to as d-type roughness, as the roughness function is thought to scale on the outer-layer length scale. The present simulations are conducted in a minimal-span channel, which explicitly limits the size of the largest length scale in the flow. By progressively widening the channel and increasing this largest length scale, it was found that there was little change to the mean velocity profile when $L_y \geq 3\mathcal{W}$, or when the critical wall-normal height $z_c = 0.4L_y \gtrsim 1.2\mathcal{W}$. This suggests that the outer layer of the flow is not significant to this rough surface, raising questions about the classification of such surfaces as d-type.

The roughness function appears to be tending towards the k-type asymptote when fixed ratios of $k/\mathcal{W}$ are considered (figure 6*a*), where each ratio of $k/\mathcal{W}$ has a different offset constant in $\kappa^{-1}\log(k^+) + D$. However, the pressure to total drag ratio and virtual origin all show little variation with k, suggesting that k is no longer relevant to the flow. A clear collapse is seen when the roughness function is instead plotted as a function of $\mathcal{W}^+$ for fixed ratios of $k/\mathcal{W} \geq 3$. The fully rough asymptote would then be $\kappa^{-1}\log(\mathcal{W}^+) + C$, where $C \approx -6.7$ and can be related to the offset D as $D = C - \kappa^{-1}\log(k/\mathcal{W})$. For a given value of $k/\mathcal{W}$, this enables the offset constant and to be calculated, and hence the equivalent sand grain roughness at given operating conditions, $k_s = \mathcal{W}\exp(\kappa(3.5+C)) \approx 0.3\mathcal{W}$. This applies for any bar roughness which has a sufficiently high aspect ratio $k/\mathcal{W} \geq 3$.

The fully rough inertial limit of $\mathcal{W}^+$ being large has yet to be been attained through numerical simulations, although would be of considerable interest. An estimate for the fully rough constant $C \approx 6.7$ has been given using the present data at $\mathcal{W}^+ = 100$, although this could be better validated with higher $\mathcal{W}^+$ values. Perry *et al.* (1969) had large $\mathcal{W}^+$ values, with $\mathcal{W}^+ \approx 250$ in the zero pressure gradient boundary layers cases and $\mathcal{W}^+ \gtrsim 1000$ in the adverse pressure gradient cases. The present values of $10 \leq \mathcal{W}^+ \leq 100$ are therefore more reminiscent of transitionally rough k-type surfaces. However, the computational requirements for simulating turbulent flow over bars with $\mathcal{W}^+ \approx 1000$, even with the minimal-span channel, are currently prohibitive.

ACKNOWLEDGEMENTS

The authors would like to acknowledge the financial support of the Australian Research Council and the Bushfire and Natural Hazards Cooperative Research Council. Computational time was granted under the Victoria Life Sciences Computational Initiative, which is supported by the Victorian Government, Australia.

REFERENCES

Ambrose, H. H. 1956 The effect of character of surface roughness on velocity distribution and boundary resistance. The University of Tennessee College of Engineering, Knoxville, Tennessee.

Chan, L., MacDonald, M., Chung, D., Hutchins, N. & Ooi, A. 2015 A systematic investigation of roughness height and wavelength in turbulent pipe flow in the transitionally rough regime. *J. Fluid Mech.* **771**, 743–777.

Chung, D., Chan, L., MacDonald, M., Hutchins, N. & Ooi, A. 2015 A fast direct numerical simulation method for characterising hydraulic roughness. *J. Fluid Mech.* **773**, 418–431.

Coleman, S. E., Nikora, V. I., McLean, S. R. & Schlicke, E. 2007 Spatially averaged turbulent flow over square ribs. *J. Eng. Mech.* **133**, 194–204.

Cui, J., Patel, V. C. & Lin, C.-L. 2003 Large-eddy simulation of turbulent flow in a channel with rib roughness. *Int. J. Heat Fluid Fl.* **24**, 372–388.

Djenidi, L., Elavarasan, R. & Antonia, R. A. 1999 The turbulent boundary layer over transverse square cavities. *J. Fluid Mech.* **395**, 271–294.

Finnigan, J. 2000 Turbulence in plant canopies. *Annu. Rev. Fluid Mech.* **32**, 519–571.

Flores, O. & Jiménez, J. 2010 Hierarchy of minimal flow units in the logarithmic layer. *Phys. Fluids* **22**, 071704.

Hama, F. R. 1954 Boundary-layer characteristics for smooth and rough surfaces. *Trans. Soc. Naval Arch. Mar. Engrs* **62**, 333–358.

Hamilton, J. M., Kim, J. & Waleffe, F. 1995 Regeneration mechanisms of near-wall turbulence structures. *J. Fluid Mech.* **287**, 317–348.

Jackson, P. S. 1981 On the displacement height in the logarithmic velocity profile. *J. Fluid Mech.* **111**, 15–25.

Jiménez, J. 2004 Turbulent flows over rough walls. *Annu. Rev. Fluid Mech.* **36**, 173–196.

Jiménez, J. & Moin, P. 1991 The minimal flow unit in near-wall turbulence. *J. Fluid Mech.* **225**, 213–240.

Leonardi, S., Orlandi, P. & Antonia, R. A. 2007 Properties of d-and k-type roughness in a turbulent channel flow. *Phys. Fluids* **19**, 125101.

MacDonald, M., Chan, L., Chung, D., Hutchins, N. & Ooi, A. 2016 Turbulent flow over transitionally rough surfaces with varying roughness density. *J. Fluid Mech.* **804**, 130–161.

MacDonald, M., Chung, D., Hutchins, N., Chan, L., Ooi, A. & García-Mayoral, R. 2017 The minimal-span channel for rough-wall turbulent flows. *J. Fluid Mech.* **816**, 5–42.

Moser, R. D., Kim, J. & Mansour, N. N. 1999 Direct numerical simulation of turbulent channel flow up to $Re_\tau = 590$. *Phys. Fluids* **11**, 943–945.

Nagib, H. M. & Chauhan, K. A. 2008 Variations of von Kármán coefficient in canonical flows. *Phys. Fluids* **20**, 101518.

Perry, A. E., Schofield, W. H. & Joubert, P. N. 1969 Rough wall turbulent boundary layers. *J. Fluid Mech.* **37**, 383–413.

Sadique, J., Yang, X. I. A., Meneveau, C. & Mittal, R. 2017 Aerodynamic properties of rough surfaces with high aspect-ratio roughness elements: Effect of aspect ratio and arrangements. *Boundary-Layer Meteorol.* **163**, 203–224.

Sams, E. W. 1952 Experimental investigation of average heat-transfer and friction coefficients for air flowing in circular tubes having square-thread-type roughness. NACA RM E52D17.

Streeter, V. L. & Chu, H. 1949 Fluid flow and heat transfer in artificially roughneed pipes. Final Report, Project 4918. Armour Research Foundation, Illinois.

Townsend, A. A. 1976 *The Structure of Turbulent Shear Flow*, 2nd edn. Cambridge Univ. Press.

Yang, X. I. A., Sadique, J., Mittal, R. & Meneveau, C. 2016 Exponential roughness layer and analytical model for turbulent boundary layer flow over rectangular-prism roughness elements. *J. Fluid Mech.* **789**, 127–165.